International Journal of Fatigue 119 (2019) 43–51

Contents lists available at ScienceDirect

International Journal of Fatigue

journal homepage: www.elsevier.com/locate/ijfatigue

Fatigue crack growth rates on the weld metal of high heat input submerged arc welding

Luiz Henrique Soares Barbosa[a,*], Paulo José Modenesi[a], Leonardo Barbosa Godefroid[b], Ariel Rodriguez Arias[a]

[a] Federal University of Minas Gerais – UFMG, 6627, Departamento de Engenharia Metalúrgica e de Materiais, Pres. Antônio Carlos Avenue, Pampulha, Belo Horizonte, MG 31270-901, Brazil
[b] Federal University of Ouro Preto – UFOP, Departamento de Engenharia Metalúrgica e de Materiais, 122, Diogo de Vasconcelos Street, Pilar, Ouro Preto, MG CEP 35400-000, Brazil

ARTICLE INFO

Keywords:
High heat input welding
Integrated cold electrode
Fatigue crack growth rate
Welding metallurgy

ABSTRACT

Submerged arc welding (SAW) with high heat input and more than one wire has been used to weld thick plates in order to reduce the number of passes and consequent increase of productivity in the shipbuilding and oil industries. Additional characteristics of SAW such as high penetration and relative ease to produce welds with good finishing and without discontinuities contribute to this process has being widely applied. However, the use of very high heat inputs leads to the formation of a large melting pool and large amount of liquid metal, and it submits the weld region to long-term thermal cycles with low cooling rates. This scenario contributes to the formation of thick solidification structures and, at the end of the cooling, results in a microstructure consisting mainly of grain boundary ferrite with low mechanical strength and large grain size. This research evaluated fatigue cracks growth rates in welding metals with heat input higher than 10 kJ/mm made of the new SAW technique, called Integrated Cold Electrode™ with addition of non-energized (cold) wire. Single pass welds were made on 25 mm thick EH36 steel varying the chemical composition of the wire (filler metal). Microstructure, mechanical properties and $da/dN \times \Delta K$ graphics were made with the propagation of the crack in the longitudinal direction of the weld. For all tested conditions, propagation rates were similar to Paris regime base metals. However, the welds presented a crack propagation threshold higher than base metal, and fatigue threshold of higher heat input welds was increased using a molybdenum-containing filler metal. It was attributed to the presence of a higher amount of acicular ferrite in this particular welding microstructure.

1. Introduction

A welded joint is by nature a critical region for fatigue cracks initiation. It is because to macro and microscopic discontinuities, which can generate stress concentrations in both the welded zone and the heat affected zone. The most common discontinuities are pores, lack of fusion and penetration, cracks formed at different welding moments, inclusions, and microstructural heterogeneity. The choice of suitable consumables, according to a welding process that guarantees greater efficiency and control has a fundamental importance to reduce the presence of these discontinuities. However, even when care is taken to minimize or prevent the formation of structural discontinuities, a welded joint is characterized by microstructural changes that depend on welding conditions and may exhibit different resistance to fatigue crack propagation.

In the heavy structures construction, reducing the number of weld passes by increasing the rate of deposition is a desirable goal for improving productivity. This reduction, however, tends to be followed by a heat input increase and consequently causes the welded joint to be subjected to longer periods at temperatures above 1200 °C and at low cooling rates. This provides formation of solidification structures with large spacing, growth of austenitic grain and the consequent development of thick structures formed predominantly by grain boundary ferrite and intragranular ferrite which tend to prejudice the mechanical properties of the weld metal [1,2]. Although these consequences, developments in the manufacture of welding steels and consumables have allowed the use of very high heat input mainly in the shipbuilding and oil industries.

* Corresponding author at: 629 Alabandina Street, Caiçara, Belo Horizonte, MG CEP 30775330, Brazil.
E-mail addresses: lhsbop@yahoo.com.br (L.H.S. Barbosa), modenesi@demet.ufmg.br (P.J. Modenesi), leonardo@demet.em.ufop.br (L.B. Godefroid), arielra@demec.ufmg.br (A.R. Arias).

https://doi.org/10.1016/j.ijfatigue.2018.09.020
Received 9 April 2018; Received in revised form 2 September 2018; Accepted 22 September 2018
Available online 26 September 2018
0142-1123/

In addition, recent advances in technologies applied to welding processes have contributed to the increase productivity, in some cases, restricting the increase of the heat input. Submerged Arc Welding is already acknowledge industrially because it allows the use of higher heat inputs than other processes commonly used, presenting variants that work with several wires and sources, maximizing the deposition rate [3].

In addition, there is also the possibility of joining non-energized wires, known as “cold wires”. Recent technology for submerged arc welding, applies to the same head two wires connected to the same power source while a cold wire is fed between. This technology is called Integrated Cold Electrode (ICE™) and it takes advantage of the heat generated in the arc between the two electrodes and the plate to melt the non-energized wire, which increases the deposition rate without increasing the heat input [4]. Thus, the cold wire feed has the potential to influence the way the heat generated by the arc is released into the melt pool, affecting the weld thermal cycle [5,6].

The welded zone in multipass welding generally has a varied and complex microstructure due to the reheating promoted by the subsequent weld passes; however, this effect does not damage the mechanical properties. A single-pass weld, therefore, will tend to present less microstructural complexity [2,5–7] but due to the higher heat input used in its production, it may present a less adequate mechanical behavior because of the formation of a thicker microstructure. As for fatigue behavior, if the microstructure of the welded zone is composed mainly by acicular ferrite, it tends to present a greater resistance to crack propagation [8]. This constituent acts blocking cracks, since it is formed by plates with grain contours of high angle that are able to deflect the cracks, which leads to a greater demand of energy for its propagation increasing, consequently increasing fatigue threshold (ΔK_{th}) [9–11].

However, there is little information about the fatigue cracks propagation on welded zone of high heat input welds, although aspects involving the general mechanical properties and fracture tenacity have already been studied [2,3,5–7]. Although the development of steels for applications involving welding of heavy structures in a single high heat input has evolved in recent decades, little is known about the development and application of consumables for such process. In this work, the welded zones of single-pass welds with heat inputs of 10.7 and 17.1 kJ/mm with the SAW-ICE process were characterized microstructurally and submitted to fatigue cracking growth rate tests, with the objective of evaluate their performance and their acceptability by the BS7910 standard [12]. In addition, it was compared the propagation of fatigue cracks in single pass high heat input welds to welded structures with smaller heat input and multipass from data available in literature.

2. Materials and experimental methods

The welded joints used in this study were obtained from three 25 mm thick of a naval steel welded by SAW ICE™ process in single pass. Base metal was an EH36 steel obtained by thermomechanical process followed by accelerated cooling and its chemical composition is shown in Table 1, which meets ASTM A131M-14 [13] standard. It is highlighted the reduced amount of S and P, which minimizes the formation of manganese sulfide particles inclusions and phosphorus segregation in austenite grain boundaries, to minimize the tendency for embrittlement phenomena and to avoid the decrease of mechanical properties of the steel. The base metal microstructure observed under the optical microscope is shown in Fig. 1. It is composed of a ferrite banding, Pearlite and bainite with a refined morphology. Ferrite, in polygonal shape, also appears with reduced grain size.

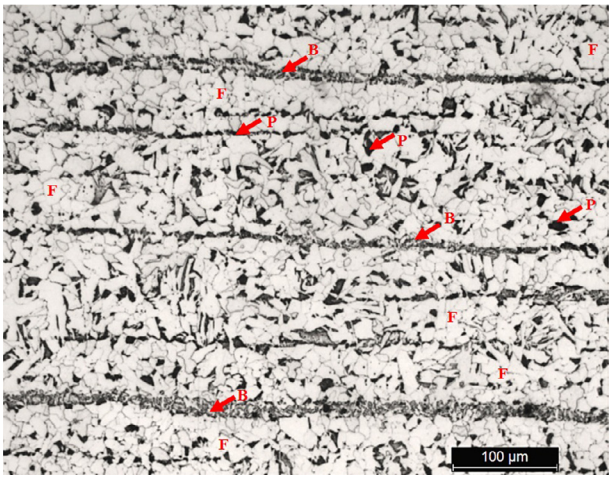

Fig. 1. Base metal microstructure in longitudinal direction of rolling. Etching nital 2%. Note: F – ferrite; B – Bainite; P – Pearlite.

The specimens were cut in 150 mm × 600 mm plates and a v-groove was machined with 10 mm opening and 8 mm of nose plus a 30° bevel angle as shown in Fig. 2. The AWS EM12K (ESAB OK Autrod 12.22) and AWS EA2 (ESAB OK Autrod 12.24) wires were used together with a basic agglomerate flow (OK Flux 10.71) as the filler metal. Table 2 shows the chemical compositions and mechanical properties typical of the filler metal according to its manufacturer [14].

Welding tests were performed with two levels of high heat input: 10.7 and 17.1 kJ/mm (considering a thermal efficiency equals to one). The welds were made with two heads, the first ICE™ with three 2.5 mm wires coupled, a cold wire and two energized by a single source operating with AC current (Twin). The other head was connected in a source operating with direct current (DC + Tandem) with a 4.0 mm diameter wire. The welding sources used are AC/DC inverters with 1000 A capacity and a 100% work cycle (Aristo 1000AC/DC). This configuration is shown in Fig. 3.

For the bigger heat input, 17.1 kJ/mm, two tests were performed. In the first one, AWS EM12K wire was used in the guide head and, in the second one, AWS EA2 wire, which has in the filler metal approximately 0.5% Mo addition and Mn content around 10% higher than EM12K. The main characteristics of the SAW process that was used are shown in Table 3. In all weld beads, a 38 mm stick-out and a cold wire feed rate of 40% of the others were maintained in the ICE™ head. In addition, after the welding processes, the slag was hold on the weld bead for 30 min, and then removed and the weld bead was cooled in the air at room temperature, around 29 °C.

Chemical analysis were performed on the weld metal by optical emission spectrometer. Samples of the weld bead cross section were mechanically polished and etching with 2% nital reagent for analysis under light microscopy and scanning electron microscopy. The microstructure characteristics of the weld zone (WZ) were observed and the

Table 1
Chemical composition of base metal (wt.%).

C	Mn	Si	P	S	Al	Cr + Ni + Mo	Nb + V + Ti	C_{eq} *	P_{cm} **
0.102	1.377	0.229	0.019	0.004	0.041	0.017	0.012	0.336	0.180

* $C_{eq.} = C + Mn/6 + (Ni + Cu)/15 + (Cr + Mo + V)/5$.
** $P_{cm} = C + Si/30 + (Mn + Cu + Cr)/20 + Ni/60 + Mo/15 + V/10 + 5B$.

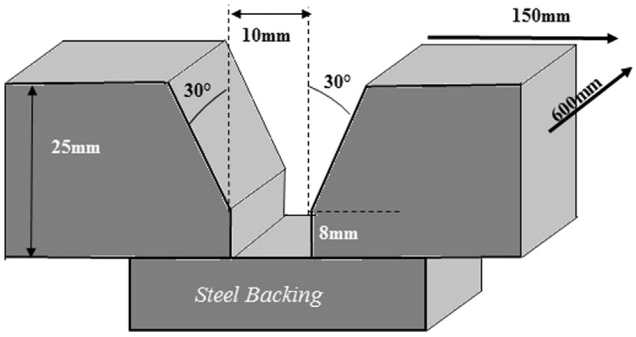

Fig. 2. Schematic design showing dimensions and shape of the groove.

Table 2
Chemical composition and mechanical properties of filler metal according to manufacturer for weld consumables [14].

Consumables (AWS A5.17)	Typical chemical composition (wt.%)	Typical mechanical properties
F48A4 - EM12K	0.05%C-0.24%Si-1.20%Mn-0.10%Cu	YS = 420; TS = 500; E = 30
F55A3 - EA2-A4	0.05%C-0.40%Si-1.40%Mn-0.50%Mo	YS = 520; TS = 590; E = 24

Note: YS – Yield Strength (MPa), TS – Tensile Strength (MPa) and E – Elongation (%).

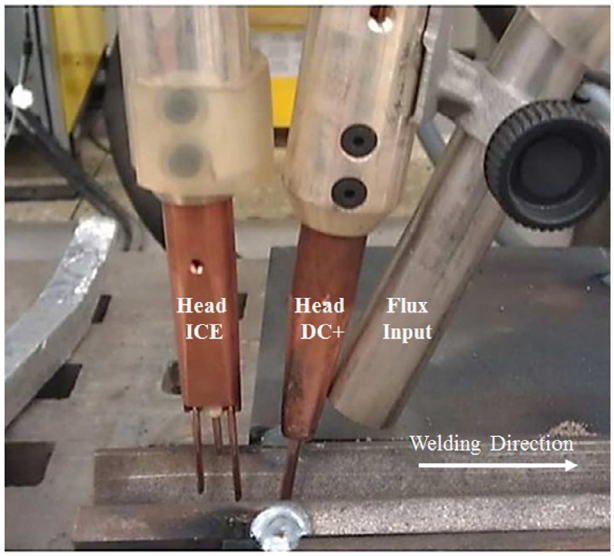

Fig. 3. Equipment configuration for high heat input SAW welding.

Table 3
Main welding parameters.

Weld bead	Head	Current (A)	Voltage (V)	Welding speed (cm/min)	Heat input (kJ/mm)
01	ICE	1000	35	40	10.7
	DC+	1000	36	40	
02	ICE	1000	35	25	17.1
	DC+	1000	36	25	
03	ICE	1000	35	25	17.1
	DC+	1000	36	25	

microstructural constituents were identified according to the International Institute of Welding (IIW) [15,16]. Quantitative metallography was performed by manual point count method provided in ASTM E562 Standard [17].

Specimens for tensile test (Fig. 4(a)) and fatigue crack propagation tests (Fig. 4(b)) were machined from the welded joints. Transverse tensile tests were performed on the weld metal and transverse to the rolling direction of the base metal according to ASTM E8M Standard [18] on an Instron model 5582 electromechanic machine of 100 kN capacity. Vickers hardness was measured with a load of 30 kgf for 15 s. The fatigue crack propagation tests were performed on an Instron 8802 servo-hydraulic machine and in accordance with ASTM E647 Standard [19], with crack propagation in the longitudinal direction of the weld bead.

Fatigue pre-cracking was performed by the constant loading method and had been used until the pre-crack length of 3 mm. The constants C and *m* of the Paris Equation were obtained by linearization of the $da/dN \times \Delta K$ curve between 1×10^{-5} and 1×10^{-3} mm/cycle. The fatigue threshold value ΔK_{th} was defined as the stress intensity factor range at which the fatigue crack growth rate decreased to below 1×10^{-7} mm/cycle. The stress ratio R and cycling frequency (*f*) were 0.1 and 30 Hz, respectively. Firstly, tests were performed in the near-threshold regime with the decreasing delta K procedure. Afterwards, the Paris regime with constant load amplitude was performed in another sample. The crack opening load (P_{op}) was estimated using a crack opening displacement (COD) compliance technique, and was assumed to be the point when the COD-load curve begins to deviate from the linear elastic curve in accordance with the recommendations of ASTM E647 Standard [19]. After the tests were completed, the fracture surfaces were examined by scanning electron microscopy.

3. Results and discussion

Table 4 shows the chemical composition of weld metal for three welding conditions discussed. Weld beads presented a chemical composition that corresponds to the filler metals used, with reduced values and very close to equivalent carbon, which also contributed to the absence of solidification cracks and cold cracking. The molybdenum content in the weld bead of 17.1 kJ/mm (EA2) was about 10 times higher than the other beads, which was already expected, since a consumable with a higher Mo content was used, the purpose of increasing the hardenability of the steel in this welded joint [20].

Metallographic observations in the welded zone without etching revealed globular inclusions composed predominantly of oxides. Under conditions of lower heat input than those used in the present work, inclusions can contribute positively to nucleation acicular ferrite [21], which has a positive role to improve the toughness and fatigue strength of the weld [22]. Fig. 5 shows the micrographs obtained for the three welding conditions and Fig. 6 shows the volumetric fraction of the main constituents present in the microstructure of the welded zone. The presence of acicular ferrite is observed in all cases despite the high heat input. The amount acicular ferrite is lower in the weld made with higher heat input without molybdenum in which it is replaced mainly by grain boundary ferrite (GF). The increase of the heat input increase acicular ferrite plates, which are converted in intragranular ferrite (IF), ferrite with the second aligned phase (FS or FS(A)) and ferrite-carbide aggregates (FC). The structures formed are thicker than structures obtained with lower heat input, as expected [1–3,6]. Other constituents can be found, such as Bainite (B), M-A (Martensite/Austenite constituent) and Pearlite (FC(P)), as showed in Fig. 5 (b), (d), (f).

The cross-tensile test results in the welded zone are summarized in Table 5. The highest values of yield strength, tensile strength and hardness were obtained in the 10.7 kJ/mm and 17.1 kJ/mm (EA2) weld beads. In the first one, because it was the one that presented the lowest heat input, it was maintained with a more refined microstructure and with a higher amount of acicular ferrite than others. In the second one, this behavior may be related to the addition of molybdenum in the weld metal that contributed to the increase of acicular ferrite in the welded zone. As for the condition of 17.1 kJ/mm, the major microstructure of primary ferrite led to a decrease in tensile strength and yield strength,

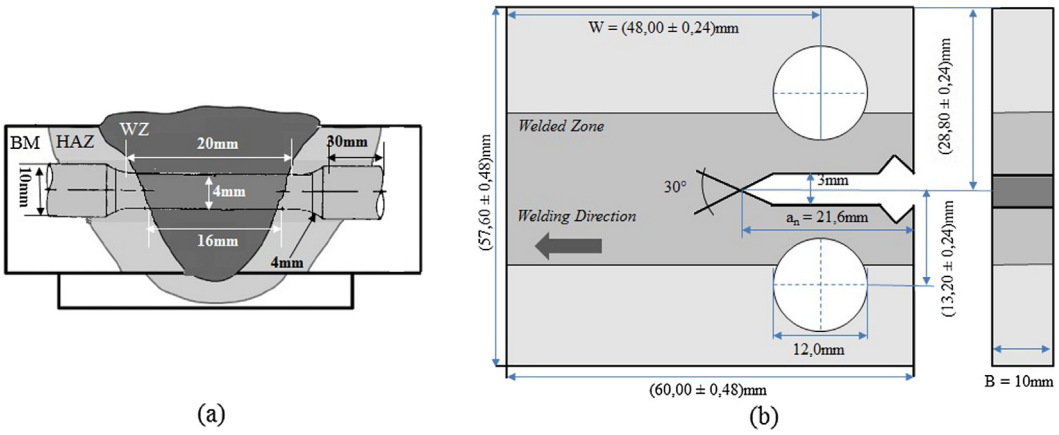

Fig. 4. Schematic representation of the test specimens dimensions (a) specimens for tensile transversal test according to ASTM E8M Standard [18] and (b) specimens for fatigue crack propagation tests according to ASTM E647 Standard [19].

consequently increasing the elongation.

From Table 5, in most cases there were overmatching, in other words the values of the yield strength of the weld metal were higher than the base metal. In this case, there will be a possibility of even higher tensile rupture on the base metal. Just the weld bead of 17.1 kJ/mm (EM12K) was undermatching.

Welded joints revealed similar fatigue crack growth rates in the Paris regime of the sigmoidal curve $da/dN \times \Delta K$, keeping slope values very close, which was expected considering that the fatigue crack growth is quite independent on microstructure in this region [23]. For fatigue threshold regime, the materials presented different behaviors according to the welding conditions applied. The results are shown in Table 6 and Fig. 7.

Fig. 7(a) shows a comparison between the base metal and the welds in which just heat input was varied. It is observed that the base metal curve presented the lowest value of ΔK_{th}. Welds usually are considered as critical regions for the development of fatigue cracks due to the presence of geometric variations and discontinuities that act as stress concentrators and the presence of residual stresses [23]. However, results indicate that the weld metals obtained with high heat input have a higher fatigue threshold; in other words they can have the propagation of the fatigue crack growth interrupted more easily.

The increase in the heat input reduced the fatigue strength in the welded zone represented by the value of ΔK_{th}. This is mainly related to the microstructure. Weld metal made with 10.7 kJ/mm, which had a higher amount of acicular ferrite than the 17.1 kJ/mm (EM12K), the value of ΔK_{th} was about 12% higher. Comparing the chemical composition, for the same contribution of 17.1 kJ/mm (Fig. 7(b)), the addition of a molybdenum-containing wire increased the ΔK_{th} by 11% for the weld metal. This variation stands because of the microstructure too, since it was the one with the highest amount of acicular ferrite among the three conditions studied. The typical morphology of acicular ferrite, which consists of the interlacing of small plates, can change the crack propagation direction, causing a greater energy consumption in this process and consequently increasing the ΔK_{th}, therefore, the increase of the volumetric fraction of ferrite acicular present in the weld zone is also responsible for the increase in fatigue crack growth resistance [10,11].

Fatigue crack closure is another factor that may explain this difference of ΔK_{th} obtained. The ASTM E647 Standard [19] makes it possible to calculate from a Load × COD curve the value of the load from which the crack will be opened (P_{op}). Thus, it is possible to obtain the P_{op}/P_{Max} ratio that corresponds to a percentage of this opening load acting on the maximum load for a given value of ΔK, obtaining the graph shown in Fig. 8.

For base metal and the heat input of 17.1 kJ/mm (EM12K), the crack closure effect was not accentuated in comparison with the others conditions, which may explain its reduced values of ΔK_{th}. The highest crack closure effects were observed on the heat inputs of 10.7 kJ/mm and 17.1 kJ/mm (EA2), which are those with the highest values of ΔK_{th}. The volumetric fraction of acicular ferrite may have influenced the process, since the crack, during its propagation, searches for regions of lower energy, in this case the primary ferrite. This makes it tortuous, favoring the roughness induced fatigue crack closure [27,29].

In this way, results of Fig. 8 may be associated with roughness-induced fatigue crack closure. Fig. 9 shown a region of the crack path near to the fatigue threshold. Acicular ferrite regions promoted greater cracking roughness than grain boundary ferrite places, showing the effect of acicular ferrite on the crack closure results for the welds with the highest amount of this constituent. In addition, for samples from 17.1 kJ/mm condition, it is noticed that the crack tends to propagate along the grain contours of the previous austenite, as also observed by Zhu et al.[29].

When this crack had to grow in AF regions, it became tortuous. Moreover, for the 17.1 kJ/mm (EM12K) condition, even though it was presented lower values of crack closure, its tendency plot is more pronounced than others, when ΔK is reduced. It may be related to the high grain size presented by this weld, also considered a relevant factor for the crack closure induced by roughness [27,29,30].

The base metal crack, shown in Fig. 9, also presented some tortuosity in the crack path, having propagated in an intergranular mode by ferrite regions in order to deviate from structures with higher resistance such as pearlite or bainite [11]. This tortuosity did not affect the fatigue crack closure. Fig. 9 shows that when the crack passes through the ferrite grain on the base metal, it presents little tortuosity, but tends to follow the grain contours, generating deviations in its way.

Table 4
Chemical composition of weld metal (wt.%).

Heat input (kJ/mm)	C	Mn	Si	P	S	Cr	Mo	Ni	Cu	V	N	Ti	C_{eq}	P_{cm}
10.7	0.102	1.292	0.301	0.022	0.009	0.037	0.010	0.009	0.034	0.003	—	0.004	0.330	0.181
17.1 (EM12K)	0.099	1.277	0.316	0.022	0.008	0.049	0.009	0.016	0.226	0.002	—	0.003	0.340	0.188
17.1 (EA2)	0.102	1.240	0.251	0.021	0.007	0.042	0.106	0.011	0.029	0.002	0.008	0.004	0.341	0.183

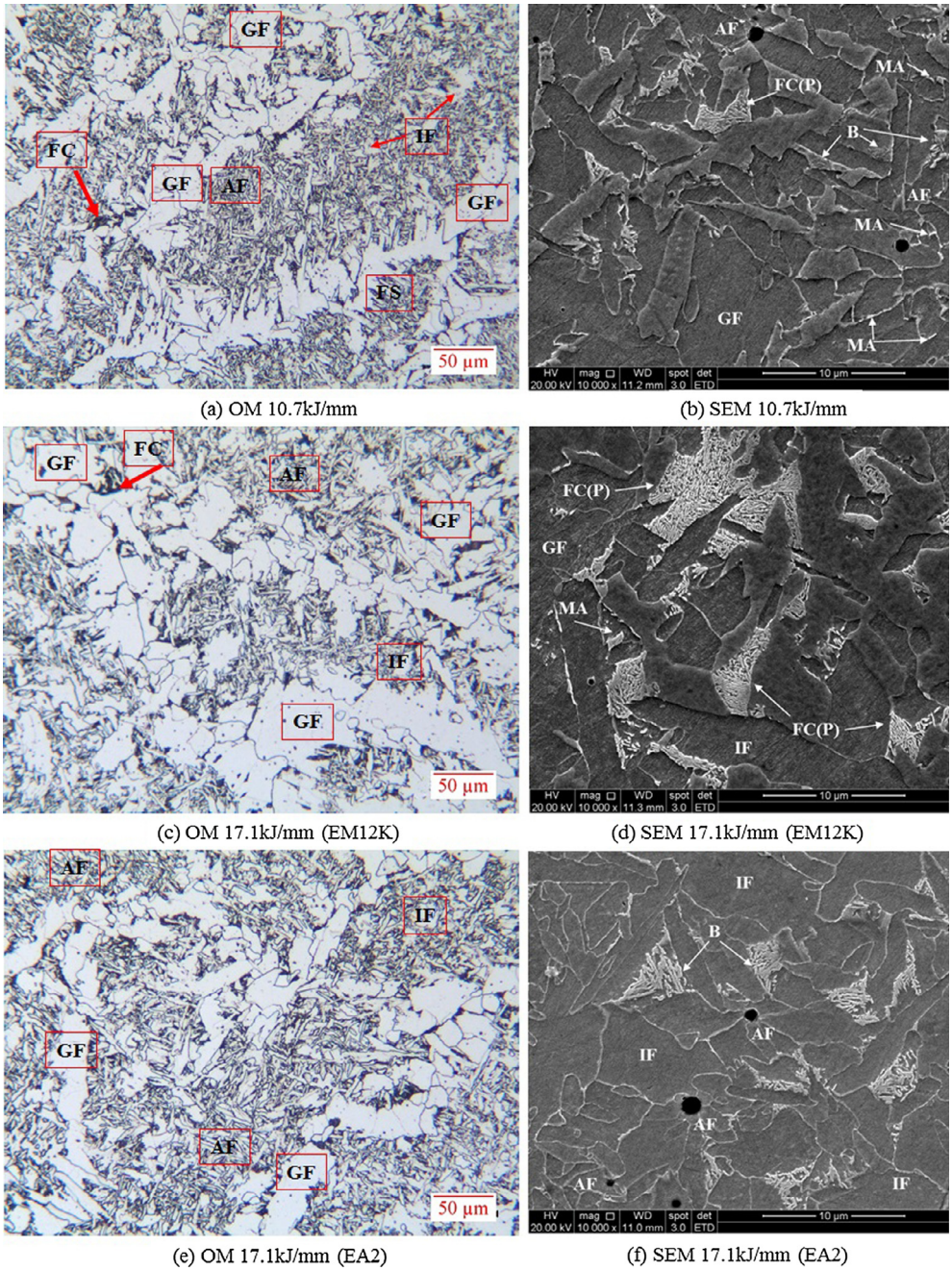

Fig. 5. Optical micrographs (a), (c), (e) and scanning electron microscopy (b), (d), (f) of welded zone for all heat inputs, etching nital 2%. Note: AF – Acicular Ferrite; GF – Grain Boundary Ferrite; IF – Intragranular Ferrite; B – Bainite; FC (P) – Pearlite; MA – Martensite/Austenite Constituent; FC – Ferrite/Carbide Aggregate; FS – Ferrite with Aligned Second Phase.

About Paris regime, results were selected of some authors [9,10,24,25,26] who studied fatigue crack propagation rates in thick joints for the shipbuilding and petroleum industries obtained with lower heat input and several weld passes. Five papers were selected following the criterion that the fatigue crack growth rate test parameters used by them were as close as possible to those used here. The consumables used by them were not taken in consideration neither were the microstructure of the welded zone after welding heat treatments. The results are shown in Table 7.

It is noted that the fatigue behavior of the welded zone on the Paris regime considering the heat inputs studied in the present work remain within a range very close to the values obtained by other authors working with lower heat inputs. This fact confirms the microstructure independence in the Paris regime and shows that the use of high heat inputs and reduction in the number of welding passes does not significantly affect fatigue behavior in this region.

Finally, as the material studied in this work applies to the shipbuilding industry, the graphs shown in Fig. 7 can be qualified according to BS7910 Standard [12], which define parameters of fatigue crack growth rates for welded and underwater structures for the naval and oil industries. The comparative curves are shown in Fig. 10. For air-welded joints subjected to a marine environment with a temperature of up to 100 °C, an extreme condition with $R \geq 0.5$ is recommended as a reference, because it has the maximum limits allowed of ΔK_{th}, C and *m*.

Note that in all welding conditions the threshold value obtained is above the referenced ΔK_{th} for both $R \geq 0.5$ where $\Delta K_{th}^{Ref} = 2\,\text{MPa.m}^{1/2}$ and for $R = 0.1$ in that $\Delta K_{th}^{Ref} = 4.7\,\text{MPa.m}^{1/2}$. Thus, it can be inferred that it is desirable to prefer a high heat input welding using a

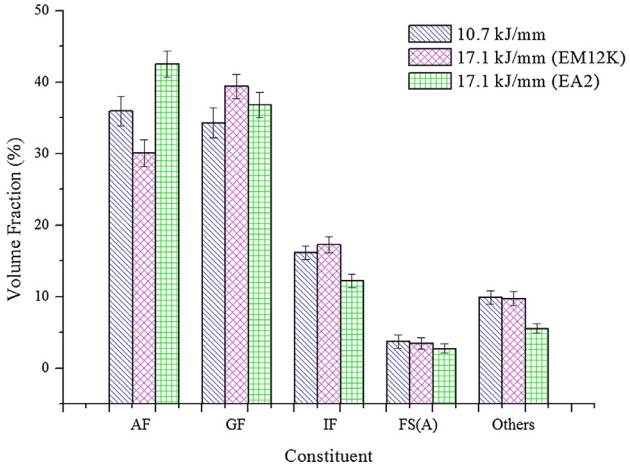

Fig. 6. Volume fraction of the main microstructural constituents.

Table 5
Basic mechanical properties of the weld metal and base metal.

HI (kJ/mm)	Y.S. (MPa)	T.S. (MPa)	Elongation %	ER (%)	$H\bar{V}3$
10.7	425 ± 2	542 ± 15	21 ± 2	78	176 ± 5
17.1 EM12K	342 ± 16	496 ± 16	25 ± 1	69	154 ± 4
17.1 EA2	422 ± 8	558 ± 10	18 ± 1	76	184 ± 6
Base Metal	375 ± 3	490 ± 8	29 ± 1	77	160 ± 5

Note: HI – Heat Input; ER – Elastic Ratio; $\bar{H}V$ – Average Vickers Hardness.

Table 6
Experimental constants of the Paris regime and threshold ΔK value.

	Paris regime		Threshold regime
Heat input (kJ/mm)	*C* (mm/cycle)	m	ΔK_{th} (MPa√m)
10.7	2.41×10^{-9}	2.99	12.3
17.1 (EM12K)	1.52×10^{-9}	3.12	10.8
17.1 (EA2)	1.88×10^{-9}	2.98	12.2
Base metal	1.98×10^{-9}	3.07	9.7

combination of wires (EM12K + EA2), that was the one that presented the best mechanical strength and fatigue resistances, meeting the requirements of BS7910 Standard [12].

Fig. 11 shows SEM fractographs obtained in the Paris regime and in the regions near to the fatigue threshold. Typical morphological characteristics are observed for each region, which depend mainly on the level of ΔK. To intermediate values of ΔK, the main characteristic to be observed is the presence of fatigue striations, resulting from the plastic blunt process at the crack tip [28]. Comparing all fractures surfaces, there were generally no differences in morphology or dimensions of fatigue striations. This also indicates the absence of possible overloads during the tests [26]. In the pictures of Fig. 9, this region was highlighted with a red rectangle.

For crack growth rates near to 10^{-7} mm/cycle, transgranular fracture characteristics are observed, in Fig. 9, showing a granulated or faceted texture throughout the image, but a small region was indicated by red circles for better viewing. Facet morphology is characteristics of lower R on the near-threshold regime [29–31] and results from changes in the orientation of the cleavage planes between grains. Moreover, faceted fracture it's related to smaller plastic zone size at the crack tip on the threshold regime [30]. Places with micro-cracks are also visible in the welded metal SEM fractographs; they are indicated with red arrows. Some present characteristics also indicate variations in the topography of the surface of this region, as small reliefs, indicated by white arrows.

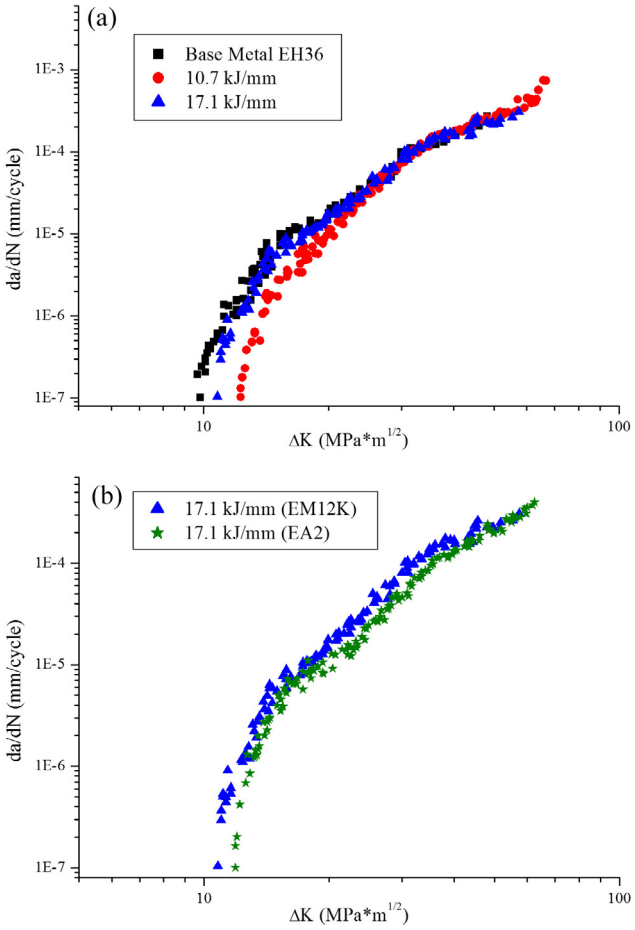

Fig. 7. Fatigue crack growth rate results; (a) effect of heat input; (b) effect of the chemical composition.

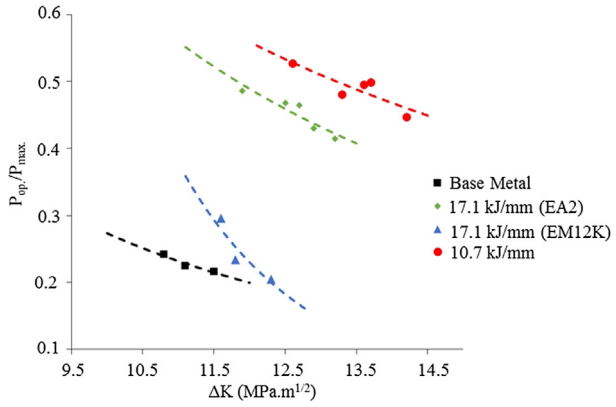

Fig. 8. Crack closure measurements for the steels studied.

4. Conclusions

A TMCP steel of naval application was welded using the submerged arc welding process with different levels of high heat input and single weld pass. In the higher heat input condition, the wire chemical composition was also varied and the obtained welded zones were subjected to fatigue crack growth rate tests. The following conclusions can be drawn from the investigation:

- The increase of heat input using the same consumables led to the formation of coarse primary ferrite with reduction of the volumetric fraction of acicular ferrite;

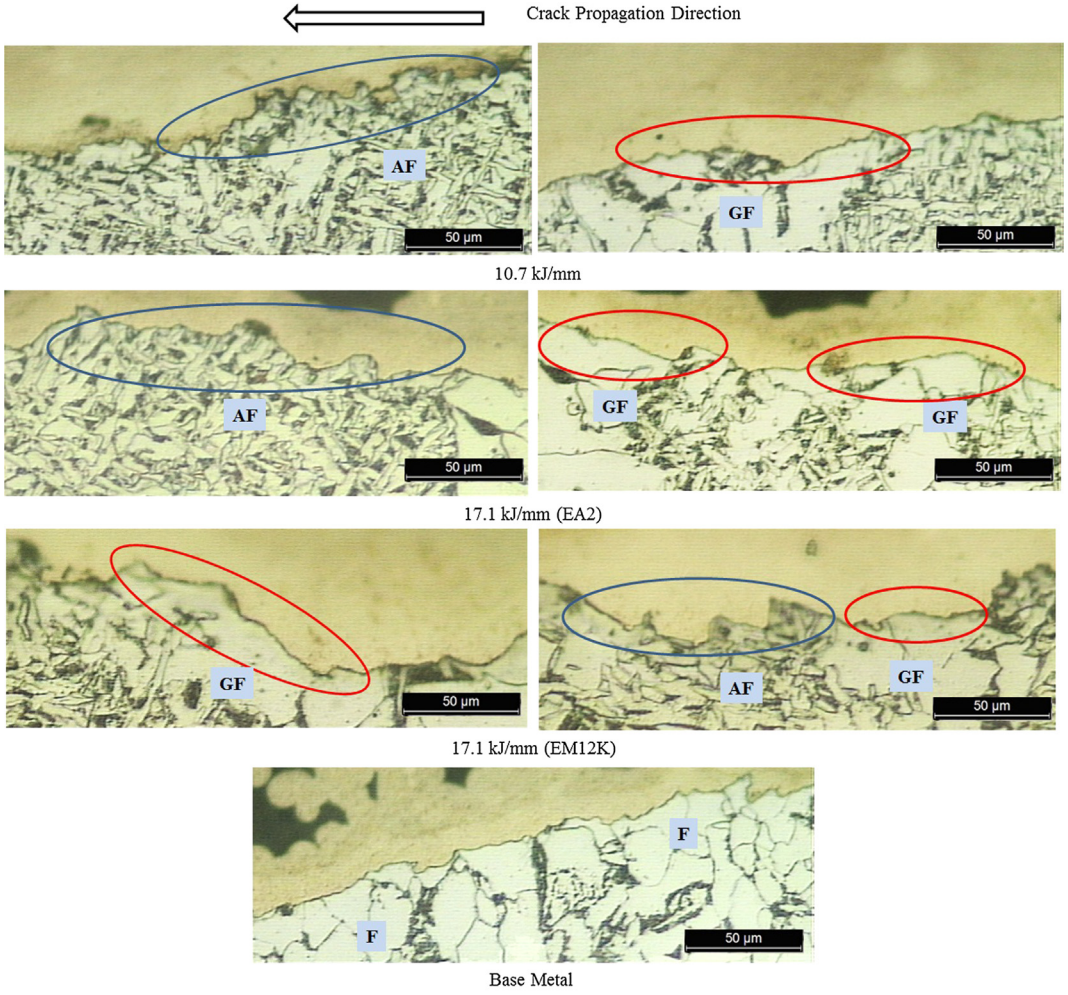

Fig. 9. Crack path on the acicular ferrite (AF) and grain boundary ferrite (GF) near to threshold. Etching nital 2%.

Table 7
Experimental values of welded-zone fatigue tests obtained from the literature.

Author(s)	Heat input kJ/mm	Number of weld passes	R	C mm/cycle	m
Tsay et al. [24]	1.48	14	0.1	2.84×10^{-10}	3.92
Braz [10] – SMAW	1.30	14	0.1	1.18×10^{-9}	2.91
Braz [10] – SAW	1.30	–	0.1	1.34×10^{-8}	2.64
Lee et al. [25]	14.90	1	0	2.33×10^{-10}	3.89
Beltrão et al.[26]	3.30	–	0.1	1.60×10^{-9}	3.22
Xiong and Hu [9]	2.40	4	0.1	7.26×10^{-9}	2.86

- When changing the wire chemical composition, adding small quantities of molybdenum, it was increased the hardenability of weld metal and acicular ferrite volume fraction remained at levels similar to those of lower heat inputs welding;
- Tension and hardness properties were reduced with the heat input increase, but the addition of a wire containing molybdenum also contributed to the maintenance of the mechanical properties in the higher heat input welding;
- Fatigue crack propagation tests have shown that the heat input effect on this property is related to the presence of acicular ferrite, which acts as regions that deflect the crack, making it tortuous and promoting roughness induced crack closure. Thus, the welding conditions that provided greater volumetric fraction of acicular ferrite were those of greater resistance to fatigue crack growth;

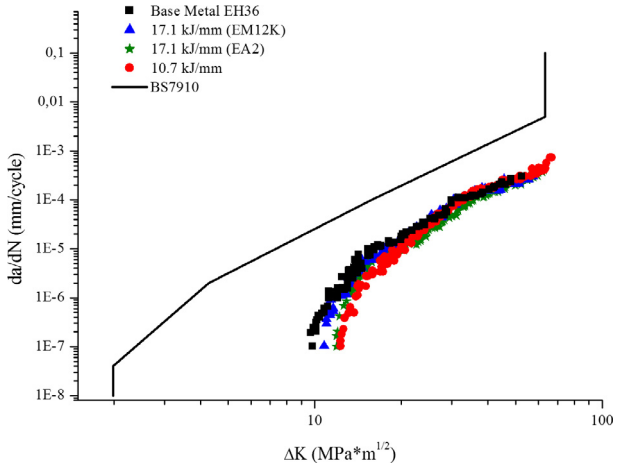

Fig. 10. Comparison between da/dN × ΔK curves obtained in this work and the BS7910 Standard [12] to R ≥ 0.5.

- Even under these extreme conditions of heat input in order to perform a single pass weld, fatigue crack propagation rates results in accordance with BS7910 Standard for naval application and present values of C and m near to those of multipass low heat inputs welding.

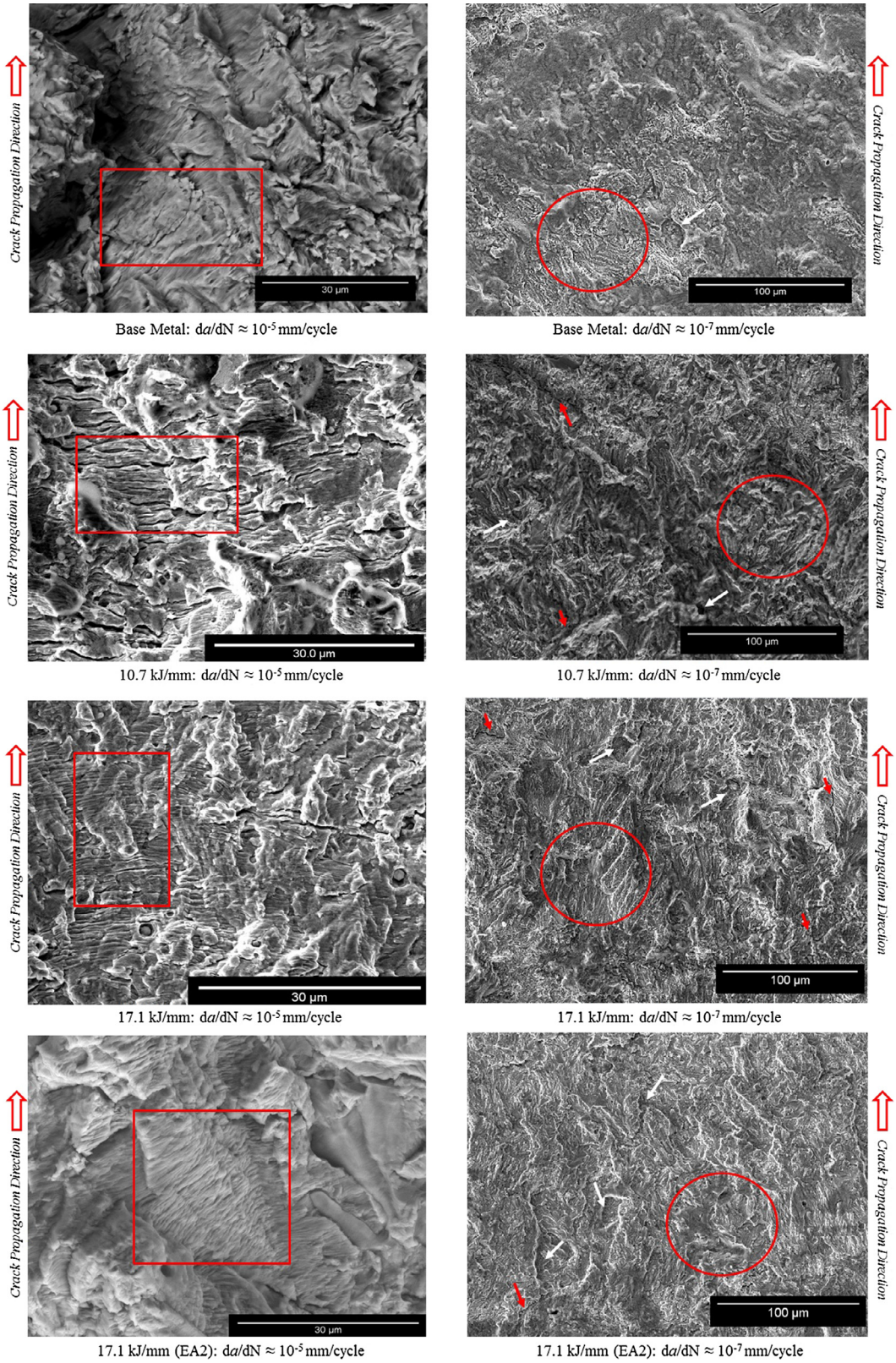

Fig. 11. SEM fractographs in two regions of da/dN × ΔK curves.

Acknowledgments

The authors thank ESAB for donation of consumables and welding, Usiminas for supplying the base metal, National Council for the Improvement of Higher Education (CAPES) by research foment, LRSS and DEMET/UFMG.

References

[1] Viano DM, Ahmed NU, Schumann GO. Influence of heat input and travel speed on

microstructure and mechanical properties of double tandem submerged arc high strength low alloy steel weldments. Sci Technol Weld Joining 2000;5(1):26–34.
[2] Jorge JCF, Souza LFG, Marouco ES, Filho ORS, Diniz JLC. Propriedades Mecânicas e Microestruturais de Juntas Soldadas pelo Processo a Arco Submerso com Elevado Aporte Térmico. Soldagem & Inspeção 2015;20(3):347–58.
[3] Layus P, et al. Multi-wire SAW of 640 MPa Arctic shipbuilding steel plates. Int J Adv Manuf Techno, Springer-Verlag, London 2014;2014(75):771–82. ISSN DOI 10.1007/s00170-014-6147-2.
[4] ESAB. Welding Equipment AB, Integrated cold electrod submerged arc welding process description. Gothenburg; 2012.
[5] Mohammadijoo M, Kenny S, Collins L, Henein H, Ivey DG. Characterization of HAZ of API X70 microalloyed steel welded by cold-wire tandem submerged arc welding. Metall Mater Trans A 2017;48A:2247–59.
[6] Borba TMD, Flores WD, Turani LO, Júnior RC. Avaliação da Soldabilidade do Aço Naval EH36 TMCP Soldado por Arco Submerso com Elevado Aporte de Calor. Soldagem & Inspeção 2015;20(1):92–104.
[7] Lan LY, et al. Effect of single pass welding heat input on microstructure and hardness of submerged arc welded high strength low carbon bainitic steel. Sci Technol Weld Join 2012;17:564–70.
[8] Zhao M-C, Yang K, Shan Y. The effects of thermo-mechanical control process on microstructures and mechanical properties of a commercial pipeline steel. Mater Sci Eng A 2002;335:14–20.
[9] Xiong Y, Hu XX. The effect of microstructures on fatigue crack growth in Q345 steel welded joint. Fatigue Fract Eng Mater Struct 2012;35:500–12.
[10] Braz MHP. Propriedades de fadiga de soldas de alta resistência e baixa liga com diferentes composições microestruturais. Dissertação de Mestrado. Universidade de São Paulo; 1999.
[11] Xiong Z, et al. The contribution of intragranular acicular ferrite microstructural constituent on impact toughness and impeding crack initiation and propagation in the heat-affected zone (HAZ) of low-carbon steels. Mater Sci Eng A 2015;636:117–23.
[12] BS7910: BS 7910:2013 + A1:2015. Guide to methods for assessing the acceptability of flaws in metallic structures. British Standards Institution [S.l.]; 2013. p. 490.
[13] ASTM A 131/131M – Standard specification for structural steel for ships. ASTM International. West Conshohocken, PA; 2014.
[14] ESAB. Catálogo de Consumíveis. Contagem – MG: ESAB; Março; 2017.
[15] IIW Sub-Commission IXJ "Guide to the light microscope examination of ferritic steel weld metals". IIW Doc. IX-1533-88; 1988.
[16] Thewlis G. Classification and quantification of microstructures in steels. Mater Sci Technol 2004;20:143–60.
[17] ASTM E562-11. Standard test method for determining volume fraction by systematic manual point count. West Conshohocken (PA): ASTM International; 2011.
[18] ASTM E8/E8M-16a. Standard test methods for tension testing of metallic materials. West Conshohocken (PA): ASTM International; 2016.
[19] ASTM E647-15. Standard test method for measurement of fatigue crack growth rates. Am Soc Test Mater [S.l.] 2015.
[20] Evans GM, Bailey N. Metallurgy of basic weld metal. New York (USA): Abington Publishing; 1997.
[21] Babu SS. The mechanism of acicular ferrite in weld deposits. Curr Opin Solid State Mater Sci 2004;8:267–78.
[22] Venkateswaran P, Raman SGS, Pathak SD. Short fatigue crack growth behaviour of a ferritic steel weld metal. Sci Technol Weld Joining 2005;10(1):95–102.
[23] Zerbst U, et al. About the fatigue crack propagation threshold of metals as a design criterion – a review. Eng Fract Mech 2016;153:190–243.
[24] Tsay LW, Chern TS, Gau CY, Yang JR. Microstructures and fatigue crack growth of EH36 TMCP steel weldments. Int J Fatigue 1999;21:857–64.
[25] Lee HK, Kim KS, Kim CM. Fracture resistance of a steel weld joint under fatigue loading. Eng Fract Mech 2000;66:403–19.
[26] Beltrao MAN, Castrodeza EM, Bastian FL. Fatigue crack propagation in API 5L X-70 pipeline steel longitudinal welded joints under constant and variable amplitudes. Fatigue Fract Eng Mater Struct 2010;34:321–8.
[27] Ritchie RO, Suresh S. Some considerations on fatigue crack closure at near-threshold stress intensities due to fracture surface morphology. Metall Trans A 1982;13A:937–40.
[28] Suresh S. Fatigue of Materials. 2ª ed. Cambridge University Press; 2004. [S.l.].
[29] Zhu Ming-Liang, Xuan Fu-Zhen, Wang Guo-Zhen. Effect of microstructure on fatigue crack propagation behavior in a steam turbine rotor steel. Mater Sci Eng A 2009;515:85–92.
[30] Zhu Ming-Liang, Xuan Fu-Zhen. Effect of microstructure on appearance of near-threshold fatigue fracture in Cr–Mo–V steel. Int J Fract 2009;159:111–20.
[31] Du Yan-Nan, Zhu Ming-Liang, Xuan Fu-Zhen. Transitional behavior of fatigue crack growth in welded joint of 25Cr2Ni2MoV steel. Eng Fract Mech 2015;144:1–15.